



Impact of ammonia addition on soot and NO/N₂O formation in methane/air co-flow diffusion flames

Yu Yang^a, Shu Zheng^{a,*}, Ran Sui^b, Qiang Lu^{a,*}

^a National Engineering Research Center of New Energy Power Generation, North China Electric Power University, Beijing 102206, China

^b Center for Combustion Energy and MoE Key Laboratory of Thermal Science and Power Engineering, Department of Energy and Power Engineering, Tsinghua University, Beijing 100084, China



ARTICLE INFO

Article history:

Received 28 April 2022

Revised 19 October 2022

Accepted 24 October 2022

Keywords:

Ammonia combustion

Co-burning of ammonia and hydrocarbons

NH₃/CH₄/air diffusion flame

Soot formation

NO emission

ABSTRACT

Ammonia (NH₃) is receiving considerable attention as a potential substitute for carbon-containing fuels to reduce CO₂ and soot emissions. Co-burning with hydrocarbons is a feasible solution to improve the combustion performance of NH₃, which however, brings new challenges such as NO emissions. Hence, it is essential to investigate the detailed suppression/formation mechanisms of soot and NO during the co-burning of NH₃ and hydrocarbons. In this study, the effects of NH₃ addition in the fuel stream on soot and NO formations in a CH₄/air co-flow atmospheric-pressure diffusion flame were numerically investigated using a 2D code and a combined chemical mechanism comprised of a model of polycyclic aromatic hydrocarbons (PAHs) up to five-rings and detailed nitrogen-containing reactions. The integral of reaction rates over the whole flame were obtained in both CH₄ and CH₄-NH₃ co-flow flames to quantitatively investigate how the NH₃ addition affected the soot and NO formation pathways. The results showed that the addition of 10% NH₃ in the fuel stream of a CH₄/air diffusion flame had a strong suppression on soot formation, decreasing the peak soot volume fractions by 38.9%. It was found that the NH₃ addition led to decreases in CH₄ and H mole fractions close to the burner exit, and hence lowered the integral of reaction rate of R67 (CH₄+H=CH₃+H₂) by 1.07×10⁻⁵ mol/s, which in turn reduced the A1 production mainly through the pathway of CH₄→CH₃→C₂H₆→C₂H₅→C₂H₄→C₂H₃→C₂H₂→C₃H₃→A1. NO and NH played an important role in the consumption of C₁~C₂ species involved in A1 formation pathways. The NH₃ addition led to an increase in the integrated rates of CH₃+NH=CH₂NH+H and C₂H+NO=HCN+CO by 2.45×10⁻⁶ and 2.59×10⁻⁶ mol/s, respectively. The decrease of A1 mole fraction reduced the inception, condensation and HACA surface growth rates. The peak NO mole fraction was increased by two orders of magnitude, from 28 ppm in the CH₄ flame to 3060 ppm in the CH₄-NH₃ flame. A promoting effect of NH₃ addition on N₂O was observed in CH₄-NH₃ mixtures, however, through different channels than that of CH₄ flames. In addition, more CN species, such as CH₂NH, H₂CH and CH₂CN, were produced in the CH₄-NH₃ flame compared to the CH₄ flame.

© 2022 The Combustion Institute. Published by Elsevier Inc. All rights reserved.

1. Introduction

Carbon-free fuels such as ammonia and hydrogen are attracting considerable attention recently in the energy industry. In comparison with H₂, NH₃ has lower vapor pressure and can be liquified at 9.9 atm and 298 K [1], making it easier and cheaper to store and transport. Furthermore, NH₃ is a potential low-cost fuel since it can be easily produced from renewable energy and nitrogen from air [2]. However, there are several crucial limitations in the utilization of NH₃ as a fuel, such as its low burning velocity [3], high

ignition temperature [4] and low combustion stability [5]. An attractive way to overcome those shortcomings is to co-burn NH₃ with hydrocarbon fuels. To this direction, Han et al. [3] showed that the maximum burning velocity could be enhanced by 340% when NH₃ is co-burned with CH₄ at a blending ratio of 0.4. Similar results have been reported by Okafor et al. [6] and Kurata et al. [7] for gas turbine combustion, which yielded significantly higher efficiency and enhanced flame stability when CH₄ was mixed with NH₃.

In addition to reduced carbon emissions, suppression of soot formation is another advantage of NH₃ co-combustion with hydrocarbon fuels. Bockhorn et al. [8] measured soot concentrations in flat premixed C₃H₈/O₂ and C₃H₈/NH₃/O₂ flames and concluded that the decrease of soot concentration was mainly attributed to

* Corresponding authors.

E-mail addresses: shuzheng@ncepu.edu.cn (S. Zheng), qianglu@mail.ustc.edu.cn (Q. Lu).

the reduction rate of nucleation, while specific chemical pathways were not identified. Recently, Bennett et al. [9] experimentally investigated laminar counterflow $\text{C}_2\text{H}_4/\text{NH}_3$ flames and measured the soot volume fractions (SVF). Their results showed that SVF was reduced by 4–6% per 1% NH_3 addition and the nitrogen containing hydrocarbon species might be responsible for SVF reduction. Montgomery et al. [10] studied $\text{NH}_3/\text{CH}_4/\text{air}$ co-flow diffusion flames and revealed the role of NH_3 -induced C_6H_6 reduction in suppressing soot formation. However, the specific pathways for NH_3 interference in the C1-C6 reactions are yet to be elucidated. An opposed-flow reactor was adopted by Liu et al. [11] to clarify the effects of NH_3 addition on PAHs formation pathways in C_2H_4 co-flow diffusion flames. They found that the decreased rate of $2\text{C}_3\text{H}_3=\text{A}1$ played a major role in the lower A1 yield and consequently inhibited the PAHs growth. Nevertheless, the soot inception, condensation, HACA surface growth and O_2/OH oxidation processes were not considered in the opposed-flow flames they used, which might exhibit different combustion characteristics compared to the co-flow flame. They also calculated the total loadings of PAHs by integrating PAHs concentration along radial and axial directions to make sure that the suppression of NH_3 on PAHs over the whole flame was taken into account. By this means the total rate of every reaction over the whole flame could also be obtained in a co-flow flame, which made it possible to perform chemical kinetic analysis for a co-flow flame. Montgomery et al. [10] and Liu et al. [11] pointed out that a large number of C1~C2 species were consumed by N-containing species to form cyanide (CN) species, which would also result in a lower loading on soot. However, little work was conducted on the effect of CN species formation on the PAHs formation pathway.

Despite NH_3 addition has significant reduction effects on soot, increased NO emission is a major penalty for NH_3 addition in hydrocarbons. Various models have been proposed to study the effect of NH_3 addition on NO formation. Li et al. [12] employed laser-saturated fluorescence (LSF) to measure NO concentration and corroborated the existence of lean NO reburning. Pathway analyses were conducted for NO formation in counterflow premixed $\text{NH}_3/\text{CH}_4/\text{air}$ flames [13] and showed that the main precursors of NO were HNO , NH_2 and CH_3 . Sullivan et al. [14] investigated NO formation in laminar $\text{CH}_4/\text{NH}_3/\text{air}$ co-flow diffusion flames and found that NO concentration increased by an order of magnitude with only 1000 ppm NH_3 addition. A similar increasing trend was also observed in laminar $\text{CH}_4/\text{NH}_3/\text{air}$ non-premixed jet flames [15]. Soot formation was not considered in these studies, which however, was reported to compete with and suppress the formation of NO [16].

The primary aim of this paper is to quantitatively explore the effect of NH_3 addition on soot formation pathways in a CH_4 co-flow diffusion flame at atmospheric pressure. The integral of reaction rates in CH_4 and $\text{CH}_4\text{-NH}_3$ flames were computed over the whole computational domain to ensure that the effect of NH_3 addition on soot formation over the whole co-flow flame was taken into account. To evaluate the effect of CN species on the PAHs formation pathway, the integral of reaction rates for CN species were also calculated. In addition, the NO formation routes were established in $\text{CH}_4\text{-NH}_3$ flames where the interactions between NO and soot were considered.

2. Numerical models

The flame code developed by Eaves et al. [17] was employed to model laminar co-flow diffusion flames in this study. A soot model that has 35 discrete sections with a constant spacing factor of 2.35 [18] was adopted. Soot formation processes including soot inception, soot surface growth and oxidation, condensation and coagulation were considered at each section. Soot inception

Table 1
Flow rates of the fuel and air streams.

Cases	CH_4 (mL/min)	NH_3 (mL/min)	Air (L/min)
1	316.8	0	50
2	316.8	35.2	50

was assumed to be the collision of five-ring PAHs (A5), such as benzo(ghi) fluoranthene (BGHIF), benzo(a)pyrene (BAPYR) and secondary benzo(a)pyrenyl (BAPYR*S), which was reported to yield better predictions compared to four-ring PAHs (A4) [19]. Soot surface growth and oxidation was modeled by the HACA mechanism [20]. The fraction of reactive soot surface sites α [21] was assumed to be $\alpha = \min[0.004\exp(10,800/T), 1.0]$ as introduced from [22]. The value of α plays a significant role in soot surface growth; however, a universal model of α has not been established. The condensation rate was calculated based on the collision between the A5 and the aggregates [23]. The condensation efficiency γ that describes the probability of sticking was set as 0.5. Coagulation was calculated based on the collision of two soot aggregates in the entire Knudsen number regime [24] with a coagulation efficiency of 0.2.

The chemical reaction mechanism used in this paper was constructed by combining the models of Glarborg et al. [25] and Chernov et al. [26]. The Glarborg mechanism describes the ammonia chemistry and interactions among C1-C2 hydrocarbons and nitrogen species, and was validated against measurements of laminar burning velocities [3] and autoignition delay times [27] in premixed $\text{CH}_4/\text{NH}_3/\text{air}$ flames. In addition, it has shown good performance in the prediction of soot formation [10,28] and NOx emission [29] in CH_4/NH_3 flames. The reaction mechanism was augmented by the soot model of Chernov, which contains reactions of C0-C5 hydrocarbons and PAHs up to five-rings (A5) and well reproduced premixed co-flow CH_4/air flames [26]. It is noted that some reactions are common in both of the base mechanisms, and only those from Chernov's model are reserved. The combined NH_3/CH_4 chemical reaction mechanism consists of 187 species and 1571 reactions and is available as supplemental materials. It is noted that there exist other recently developed reaction mechanisms, such as [30,31], which may be also suited for this work and reveal similar physics.

The radiation model includes radiative properties of the medium and a solution method for radiative heat transfer equations (RTEs). The radiative properties of CO, CO_2 , H_2O and NH_3 were obtained via the statistical narrow-band correlated- k method (SNBCK) with 9 bands ranging $150\sim9300\text{ cm}^{-1}$, which was developed in [32]. It is worth noting that few studies have taken the radiation of NH_3 into consideration in a two-dimensional co-flow flame. The absorption coefficient of soot was calculated based on Rayleigh expression [33] as $\kappa_s = 5.5f_v\eta$, where f_v is the SVF and η the wavenumber at the band center. The discrete ordinate method (DOM) with T3 quadrature scheme [34] was used to solve the RTE in two-dimensional axisymmetric cylindrical coordinates. The radiation and soot models have been applied and validated in our previous works on CH_4 and $\text{C}_2\text{H}_4/\text{C}_2\text{H}_2$ flames [35,36].

3. Computational details and model validation

2D simulations were performed to study atmospheric pressure laminar co-flow CH_4/air and $\text{NH}_3/\text{CH}_4/\text{air}$ diffusion flames in the Yale burner [37], which has a diameter of 11 mm for the fuel tube and an inner diameter of 102 mm for the concentric annular air flow. Flow rates of the fuels and air are listed in Table 1. The flow rates of CH_4 and air are 316.8 mL/min and 50 L/min in both CH_4 and $\text{CH}_4\text{-NH}_3$ flames. NH_3 with a flow rate of 35.2 mL/min was added into the fuel stream to generate a $\text{CH}_4\text{-NH}_3$ flame, which

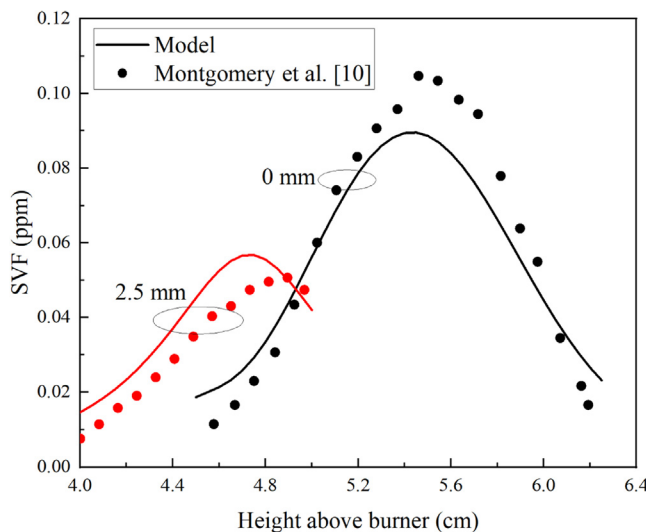


Fig. 1. SVF distributions of Case 2: predicted (lines) in this work and the measurements (symbols) [10] along the axial direction ($-z$) at two radial locations of $r = 0$ and 2.5 mm.

was identical to the set up in [10]. The exit temperatures of both streams were set as 298 K.

The computational domain of the co-flow flames was 3.78 cm (radial direction, $-r$) \times 11.56 cm (streamwise direction, $-z$) with 80 ($-r$) \times 160 ($-z$) control volumes. Non-uniform grids were used, and the minimal spatial resolutions of the mesh were 0.2 mm and 0.3 mm in the radial and streamwise directions, respectively. Grid sensitivity tests verified that further refinement of the mesh did not result in any change in the results. When the maximum relative variation of SVF over 100 iterations was less than 1×10^{-4} , iterations were considered as converged.

Figure 1 shows predicted SVFs and the corresponding measurements by Montgomery et al. [10] of Case 2 along the axial direction at two radial locations of $r = 0$ (centerline) and 2.5 mm (flame wing region). It can be observed that the predicted SVF axial ($-z$) distributions at the two radial locations well captured the experimental results. Characteristically, the highest predicted SVF along the centerline was 0.085 ppm, close to the measured 0.105 ppm. In the flame wing region, the predicted SVF distribution was also in line with the measurements. The maximal predicted and measured SVFs were 0.057 ppm at $z = 4.75$ cm and 0.050 ppm at $z = 4.9$ cm, respectively.

As a key building block for large PAHs and soot, A1's simulated mole fractions along the centerline are compared with literature experimental data from [10] and compared in Fig. 2. A case of CH₄:NH₃ vol. ratio 8:2 was calculated and compared in Fig. 2. The simulations generally well captured the peak position of A1 mole fraction and its trend as a function of vertical position, and agreed with the experimental data at height below 4 cm. The differences between the simulations and the measurements became progressively aggravated at higher positions. Nonetheless, such discrepancies were also reported in [10] and might be attributed to the original model or experimental uncertainties.

4. Results and discussion

4.1. Effects of NH₃ addition on soot formation

Simulated 2D temperature distributions and peak temperatures of CH₄ and CH₄-NH₃ flames are compared in Fig. 3. In Fig. 3(a) and (b), little difference can be found between the temperature distribution of the CH₄ and CH₄-NH₃ flames. The peak temperature fell

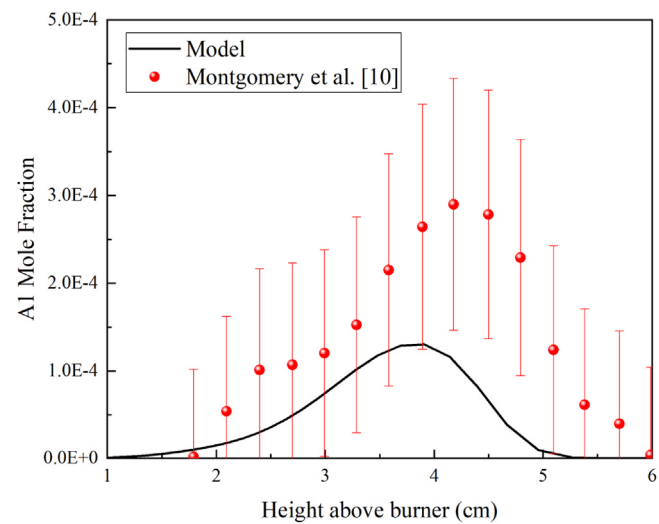


Fig. 2. A1 mole fractions along the centerline of a CH₄-NH₃ flame (CH₄/NH₃ = 0.8/0.2, fuel flow rate 377.1 mL/min): predictions (curve) in this work and measurements (symbols with error bars, [10]).

from 1998.2 K in the CH₄ flame to 1994.1 K in the CH₄-NH₃ flame, with a drop of 4.1 K. This implies the addition of 10% NH₃ had negligible impact on the temperature distribution and the peak temperature.

SVF distributions of the two different flames are presented in Fig. 4. As manifested by Fig. 4(a) and (b), soot formation was greatly suppressed by the addition of NH₃, with the maximum SVF decreased from 0.162 to 0.099 ppm (by 38.9%). Considering the NH₃ addition in the fuel stream was only 11.1% volumetrically, the much stronger (38.9%) suppression of peak SVF clearly reflects a heavy influence of NH₃ addition on soot formation. Since the soot formation consisted of four processes, i.e., soot inception, condensation, HACA surface growth and soot oxidation, it is necessary to individually reveal the impact of NH₃ addition on the four steps, which are discussed in the following sub-sections. To quantitatively discover the effect of NH₃ addition on soot production and oxidation processes at different locations (heights, $-z$) of the flame, radially-integrated rate of every process over selected flame cross-section was obtained by:

$$\alpha = 2\pi \int S r dr \quad (1)$$

Where S is the rate of inception (IN), condensation (CO), HACA surface growth (HACA) and O₂/OH oxidation processes at the given location, and r is the radial position.

4.1.1. on soot inception

Soot inception is the initial step in soot formation and has a significant impact on the other soot formation and oxidation steps [26]. The α_{IN} of CH₄ and CH₄-NH₃ flames are presented in Fig. 5. As shown, the soot inception was initiated at the height of 1 cm and vanished at 5 cm in both the CH₄ and the CH₄-NH₃ flames. The NH₃ addition led to the decrease of peak α_{IN} from 1.82×10^{-8} to 1.57×10^{-8} g/cm/s by 13.7%. Moreover, although the NH₃ addition generally reduced the soot inception, it slightly shifted the inception curve upward, resulting in greater α_{IN} at $z > \sim 4$ cm. This was also supported by the elevated SVF peak from 5.3 cm in the CH₄ flame to 5.6 cm in the CH₄-NH₃ flame (see Fig. 4).

The soot inception was modelled by the collision between two 5-ring PAHs (A5s) in this study, including BGHIF, BAPYR and BAPYR* S . The inception rate is proportional to the concentration of the colliding PAHs [20]. Figure 6 shows the distributions of

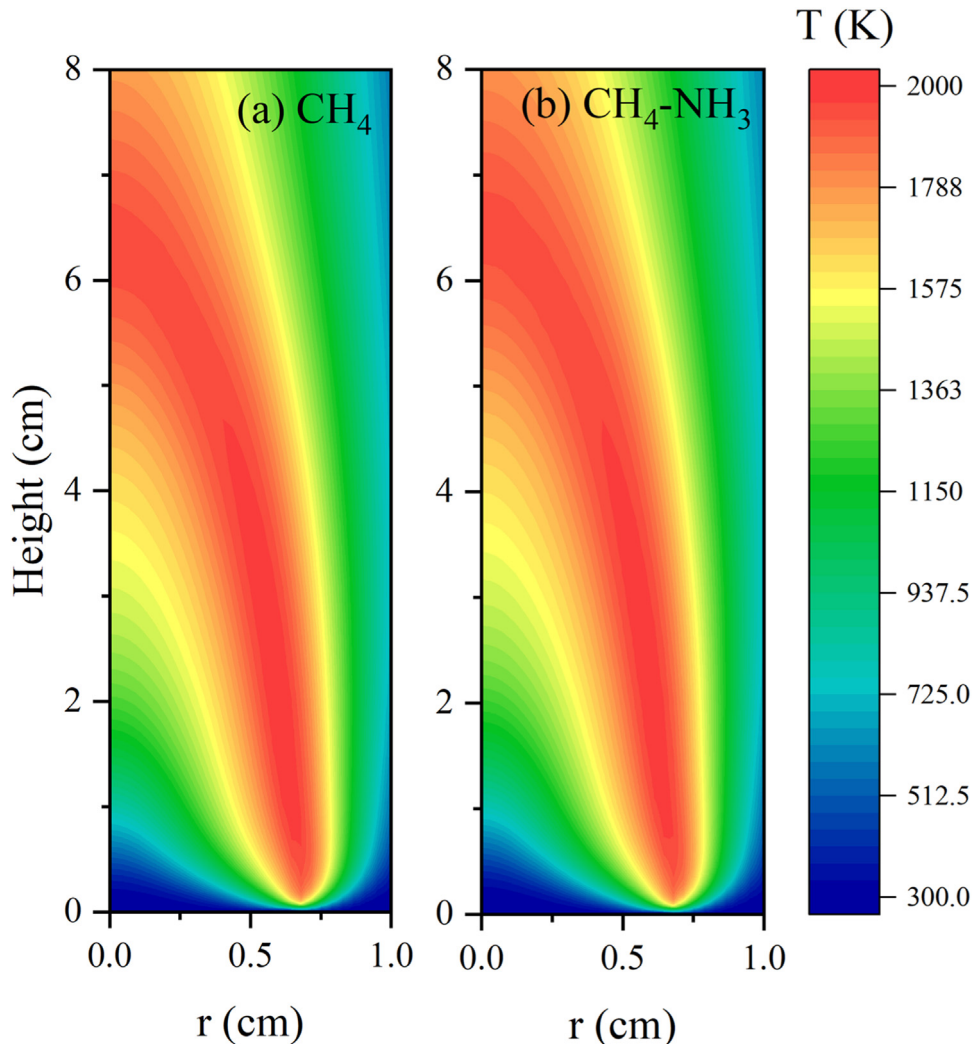


Fig. 3. Temperature distributions of (a) CH₄ and (b) CH₄-NH₃ flames. Peak temperatures are 1998.2 and 1994.1 K for the CH₄ and CH₄-NH₃ flames, respectively.

radially-integrated mole fractions (β , cm²) of the three A5s:

$$\beta = 2\pi \int f r dr \quad (2)$$

where f is the mole fraction of species at the given vertical location. It is shown that the locations of peak values of all the A5s shifted to higher locations as NH₃ was added to the CH₄ flame, which was consistent to the α_{IN} shown in Fig. 5. The NH₃ addition caused the β_{BGHIF} and β_{BAPYR} peaks to decrease by 6.62% and 14.4%, respectively. However, the impact on the peak value of β_{BAPYR^*S} was minimal. In addition, the peak values of β_{BGHIF} and β_{BAPYR} were 3 orders of magnitude higher than that of β_{BAPYR^*S} . It can thus be concluded that β_{BGHIF} and β_{BAPYR} were the two major factors in the decrease of soot inception when NH₃ was added. The formation of A5 is mainly through A1 (C₆H₆) H-abstraction and C₂H₂-addition reactions (HACA mechanism) and thus A1 is considered a significant precursor for A5 [20]. For this reason, the following discussion focuses on the effect of NH₃ addition on A1 formation.

The radially-integrated mole fractions of A1 (β_{A1}) in the CH₄ and CH₄-NH₃ flames are plotted in Fig. 7(a), which shows a decline in the peak value from 4.43×10^{-5} to 3.81×10^{-5} cm² (by 13.9%) with NH₃ addition, similar to the observations for β_{BGHIF} and β_{BAPYR} . To some extent, it reflects the dependence of A5 formation on A1 mole fraction. The A1 formation involves hundreds

of reactions (see the reaction mechanism in the supplemental material) and NH₃-addition's impact on the decline of β_{A1} should be essentially attributed to changed reaction rates of these reactions. To further quantitatively understand the effect of NH₃ addition on the reactions involved in A1 formation, the integral of reaction rates over the whole computational domain (γ , mol/s) were calculated by:

$$\gamma = \int_0^h \int_0^r 2\pi S_{rop} r dr dh \quad (3)$$

where S_{rop} is the reaction rate at the selected vertical location. The influence of NH₃ addition on A1 formation pathways can be depicted based on those γ with the biggest difference between CH₄ and CH₄-NH₃ flames. It should be stressed that what plays the decisive role in the drop of A1 formation is the γ with the biggest difference between CH₄ and CH₄-NH₃ flames, rather than the largest γ in CH₄ or CH₄-NH₃ flames.

The γ involved in A1 formation for CH₄ and CH₄-NH₃ flames are summarized in Table 2. It is noted that there were many reactions participating in the formation of each species. However, only the reactions with a relative high ratio of $\Delta\gamma$ to total $\Delta\gamma$ ($\Delta\gamma = \gamma_{CH4-NH3} - \gamma_{CH4}$) are listed. The A1 formation reactions are firstly listed in Table 2. C₃H₃ and C₃H₄ are the two main reactants in the A1 formation reactions and their formation reactions are then presented afterwards. By analogy, all the species along with

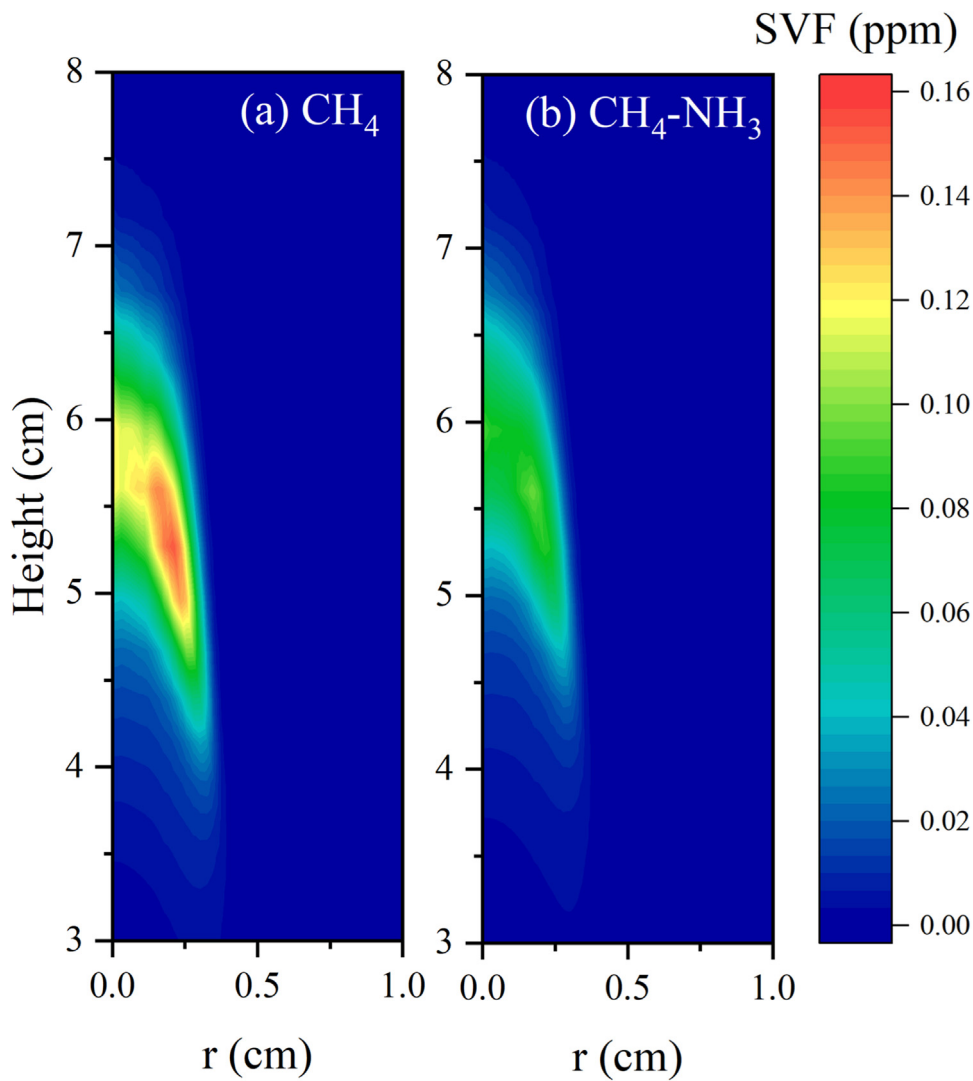


Fig. 4. SVF distributions of (a) CH_4 and (b) $\text{CH}_4\text{-NH}_3$ flames. Peak SVFs are 0.162 and 0.099 ppm for CH_4 and $\text{CH}_4\text{-NH}_3$ flames, respectively.

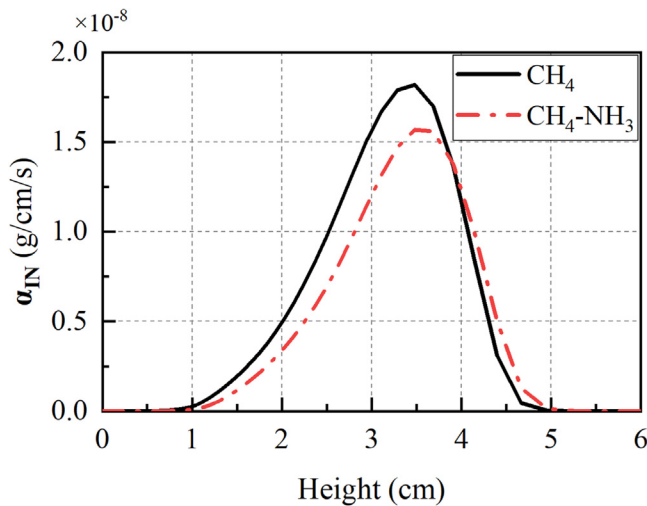


Fig. 5. The distributions of α_{IN} of CH_4 and $\text{CH}_4\text{-NH}_3$ flames.

their formation reactions playing a significant role in A1 formation can be summarized in Table 2. In addition, the radially-integrated mole fractions (β) of species shown in Table 2 are depicted in Fig. 7.

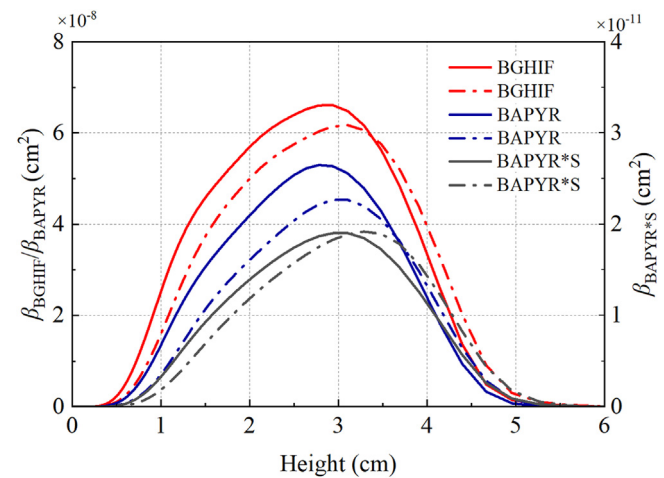


Fig. 6. The distribution of β of BGHIF, BAPYR and BAPYR*S, the solid line represents the β of CH_4 flame and dot dash line represents the β of $\text{CH}_4\text{-NH}_3$ flame.

As illustrated in Table 2, the NH_3 addition reduced γ of the combination reaction $\text{C}_3\text{H}_3+\text{C}_3\text{H}_3$ (R469) by 5.15×10^{-8} mol/s from 4.04×10^{-7} to 3.52×10^{-7} mol/s. $\Delta\gamma/\Delta\gamma_{\text{total}}$ of R469 was above 90%, which indicated that this reaction was the most significant

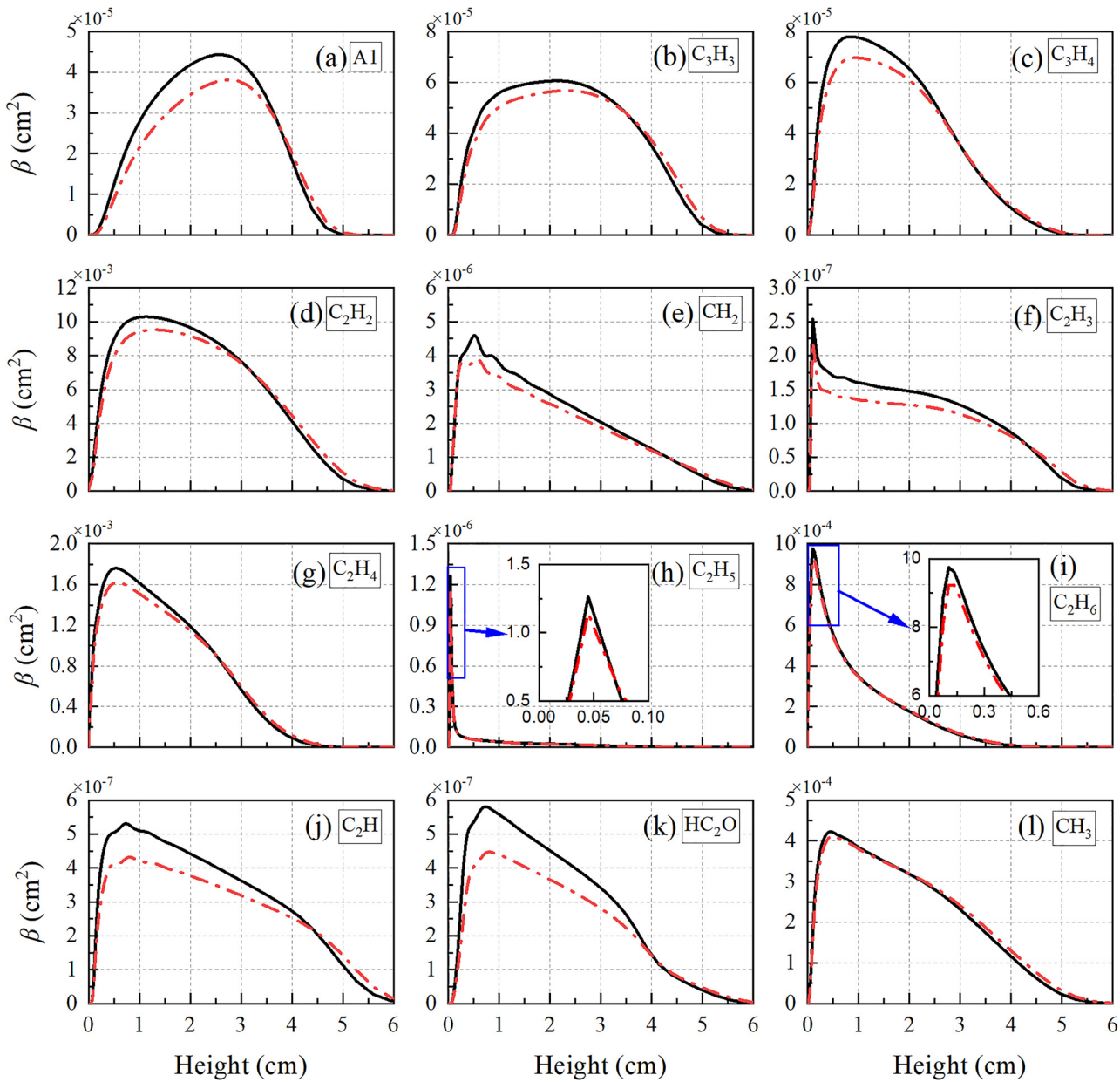


Fig. 7. Radially-integrated mole fractions (β) of species involved in A1 formation. The solid lines represent β of the CH_4 flame and the dot dash line β of the $\text{CH}_4\text{-NH}_3$ flame.

one accounting for the decline of $\beta_{\text{A}1}$. The combination reaction $\text{C}_3\text{H}_3+\text{C}_3\text{H}_4$ (R473) was also responsible for the decline of $\beta_{\text{A}1}$ but with a much smaller $\Delta\gamma/\Delta\gamma_{\text{total}}$ less than 8%.

In R469 and R473, C_3H_3 and C_3H_4 are the two main reactants and $\beta_{\text{C}_3\text{H}_3}$ and $\beta_{\text{C}_3\text{H}_4}$ are depicted in Fig. 7(b) and (c), respectively. It can be seen from Fig. 7(b) that the peak $\beta_{\text{C}_3\text{H}_3}$ decreased from 6.06×10^{-5} to 5.69×10^{-5} cm² with NH_3 addition. The combination reaction $\text{C}_2\text{H}_2+\text{CH}_2(\text{S})$ (R80) played the dominant role in the decline of $\beta_{\text{C}_3\text{H}_3}$, as manifested by the highest $\Delta\gamma/\Delta\gamma_{\text{total}}$ 57.45%. In addition, the H-abstraction of C_3H_4 (R253) and the combination reaction $\text{C}_2\text{H}_2+\text{CH}_2$ (R196) had impact on the decline of $\beta_{\text{C}_3\text{H}_3}$, with their $\Delta\gamma/\Delta\gamma_{\text{total}}$ 17.98 and 15.25%, respectively. In Fig. 7(c), the peak $\beta_{\text{C}_3\text{H}_4}$ was also lowered from 7.80×10^{-5} in CH_4 flame to 6.97×10^{-5} cm² in $\text{CH}_4\text{-NH}_3$ flame. γ of the combination reaction $\text{C}_2\text{H}_2+\text{CH}_2$ (R79) decreased by 5.89×10^{-7} mol/s and it was the only significant reaction contributing to the decline of $\beta_{\text{C}_3\text{H}_4}$.

In the formation reactions of C_3H_3 and C_3H_4 shown in Table 2, C_2H_2 and CH_2 were the essential reactants and $\beta_{\text{C}_2\text{H}_2}$ and β_{CH_2} are depicted in Fig. 7(d) and (e), respectively. As expected, the addition of NH_3 resulted in clear decreases of $\beta_{\text{C}_2\text{H}_2}$ and β_{CH_2} . γ of the decomposition reaction $\text{C}_2\text{H}_3(+M)=\text{C}_2\text{H}_2+\text{H}(+M)$ (R77) decreased by 6.54×10^{-6} mol/s with NH_3 addition, which was the dominant reaction accounting for the decrease in $\beta_{\text{C}_2\text{H}_2}$. For the formation reactions of CH_2 , γ of $\text{C}_2\text{H}_2+\text{O}$ (R390) and $\text{H}+\text{HC}_2\text{O}$ (R145) decreased by 1.88×10^{-6} and 1.08×10^{-6} mol/s respectively, which mainly contributed to the decline in β_{CH_2} .

C_2H_2 was produced via C_2H_3 , C_2H_4 , C_2H_5 and C_2H_6 successively. β of these C2 species predicted for the CH_4 and $\text{CH}_4\text{-NH}_3$ flames are plotted in Fig. 7(f-i). The H-abstraction reactions of C_2H_4 through H and OH radical (R225 and R226), with $\Delta\gamma/\Delta\gamma_{\text{total}}$ of 32.48 and 25.95%, had a significant effect on the decline of $\beta_{\text{C}_2\text{H}_3}$. C_3H_3 attacked by OH radical to yield C_2H_3 (R241) also played an

Table 2

The species and the integrated reaction rates (γ) involved in the A1 formation in CH_4 and $\text{CH}_4\text{-NH}_3$ flames.

Species	Chemical Reaction	γ_{CH_4} (mol/s)	$\gamma_{\text{CH}_4\text{-NH}_3}$ (mol/s)	$\Delta\gamma$	$\Delta\gamma/\Delta\gamma_{\text{total}}$
A1	R469: $\text{C}_3\text{H}_3 + \text{C}_3\text{H}_3 = \text{A1}$	4.04×10^{-7}	3.52×10^{-7}	-5.15×10^{-8}	90.29
	R473: $\text{C}_3\text{H}_3 + \text{C}_3\text{H}_4 = \text{A1} + \text{H}$	3.13×10^{-8}	2.68×10^{-8}	-4.50×10^{-9}	7.89
C_3H_3	R80: $\text{C}_2\text{H}_2 + \text{CH}_2(\text{S}) = \text{C}_3\text{H}_3 + \text{H}$	1.39×10^{-5}	1.17×10^{-5}	-2.23×10^{-6}	57.45
	R253: $\text{C}_3\text{H}_4 + \text{H} = \text{C}_3\text{H}_3 + \text{H}_2$	2.86×10^{-6}	2.17×10^{-6}	-6.98×10^{-7}	17.98
	R196: $\text{C}_2\text{H}_2 + \text{CH}_2 = \text{C}_3\text{H}_3 + \text{H}$	3.67×10^{-6}	3.08×10^{-6}	-5.92×10^{-7}	15.25
C_3H_4	R79: $\text{C}_2\text{H}_2 + \text{CH}_2 = \text{C}_3\text{H}_4$	3.57×10^{-6}	2.98×10^{-6}	-5.89×10^{-7}	67.04
				-8.79×10^{-7}	
C_2H_2	R77: $\text{C}_2\text{H}_3(+M) = \text{C}_2\text{H}_2 + \text{H}(+M)$	7.18×10^{-5}	6.53×10^{-5}	-6.54×10^{-6}	59.14
		-1.11×10^{-5}			
C_2H_3	R225: $\text{C}_2\text{H}_4 + \text{H} = \text{C}_2\text{H}_3 + \text{H}_2$	1.70×10^{-5}	1.49×10^{-5}	-2.19×10^{-6}	32.48
	R241: $\text{C}_3\text{H}_3 + \text{OH} = \text{HCO} + \text{C}_2\text{H}_3$	1.94×10^{-5}	1.73×10^{-5}	-2.08×10^{-6}	30.85
	R226: $\text{C}_2\text{H}_4 + \text{OH} = \text{C}_2\text{H}_3 + \text{H}_2\text{O}$	2.82×10^{-5}	2.65×10^{-5}	-1.75×10^{-6}	25.95
C_2H_4	R84: $\text{C}_2\text{H}_5(+M) = \text{C}_2\text{H}_4 + \text{H}(+M)$	4.82×10^{-5}	4.59×10^{-5}	-2.34×10^{-6}	50.47
		7.89×10^{-6}	6.68×10^{-6}	-1.20×10^{-6}	25.88
C_2H_5	R92: $\text{C}_2\text{H}_6 + \text{H} = \text{C}_2\text{H}_5 + \text{H}_2$	7.07×10^{-6}	6.15×10^{-6}	-9.21×10^{-7}	35.71
		1.92×10^{-5}	1.84×10^{-5}	-8.71×10^{-7}	33.77
C_2H_6	R187: $2\text{CH}_3(+M) = \text{C}_2\text{H}_6(+M)$	1.61×10^{-5}	1.46×10^{-5}	-1.50×10^{-6}	100.0
				-1.50×10^{-6}	
CH_3	R67: $\text{CH}_4 + \text{H} = \text{CH}_3 + \text{H}_2$	1.63×10^{-4}	1.52×10^{-4}	-1.07×10^{-5}	82.27
				-1.30×10^{-5}	
CH_2	R390: $\text{C}_2\text{H}_2 + \text{O} = \text{CH}_2 + \text{CO}$	1.27×10^{-5}	1.08×10^{-5}	-1.88×10^{-6}	50.02
		4.07×10^{-6}	2.99×10^{-6}	-1.08×10^{-6}	28.73
HC_2O	R168: $\text{C}_2\text{H} + \text{OH} = \text{HC}_2\text{O} + \text{H}$	2.16×10^{-6}	1.77×10^{-6}	-3.94×10^{-7}	38.97
		1.84×10^{-6}	1.56×10^{-6}	-2.73×10^{-7}	27.00
C_2H	R82: $\text{C}_2\text{H}_2 + \text{OH} = \text{C}_2\text{H} + \text{H}_2\text{O}$	3.21×10^{-5}	3.16×10^{-5}	-1.01×10^{-6}	48.18
				-4.47×10^{-7}	
				-9.28×10^{-7}	

important role in the decline of $\beta_{\text{C}_2\text{H}_3}$. As for C_2H_4 , there were two primary channels that contributed to the decline of $\beta_{\text{C}_2\text{H}_4}$. One was C_2H_5 decomposition reaction (R84) and the other one the combination reaction of CH_2 and CH_3 (R152). The decline of $\beta_{\text{C}_2\text{H}_5}$ was primarily due to the decrease of γ_{R92} and γ_{R141} , both by around 9×10^{-7} mol/s. The combination reaction $2\text{CH}_3(+M) = \text{C}_2\text{H}_6(+M)$ (R187) was responsible for the decline of $\beta_{\text{C}_2\text{H}_6}$. The γ_{R187} fell from 1.61×10^{-5} to 1.46×10^{-5} mol/s, with $\Delta\gamma/\Delta\gamma_{\text{total}}$ of around 100%.

As shown in Table 2, C_2H , HC_2O and CH_3 also had significant roles on the A1 formation. The $\beta_{\text{C}_2\text{H}}$, $\beta_{\text{HC}_2\text{O}}$ and β_{CH_3} were plotted in Fig. 7(j-l). As can be seen in Fig. 7(j), the peak $\beta_{\text{C}_2\text{H}}$ fell from 5.31×10^{-7} to 4.32×10^{-7} cm², with a drop of 18.6% when NH_3 was added to the CH_4 flame. That was mainly because of the decrease of γ_{R82} ($\text{C}_2\text{H}_2 + \text{OH} = \text{C}_2\text{H} + \text{H}_2\text{O}$) from 3.21×10^{-5} mol/s in the CH_4 flame to 3.16×10^{-5} mol/s in the $\text{CH}_4\text{-NH}_3$ flame. A clear decrease can be found (see Fig. 7(k)) for the peak $\beta_{\text{HC}_2\text{O}}$ from 5.81×10^{-7} to 4.47×10^{-7} cm², a drop of 23.1% with NH_3 addition. R168 ($\text{C}_2\text{H} + \text{OH} = \text{HC}_2\text{O} + \text{H}$) and R389 ($\text{C}_2\text{H}_2 + \text{O} = \text{HC}_2\text{O} + \text{H}$) were two primary reactions that contributed to the decline of $\beta_{\text{HC}_2\text{O}}$. In Fig. 7(l), β_{CH_3} close to the burner exit decreased with NH_3 addition. The H-abstraction reaction of CH_4 (R67) played the most important role in the decline of β_{CH_3} , with $\Delta\gamma/\Delta\gamma_{\text{total}}$ of 82.27%. Two reasons can be found for illustrating the decline of γ_{R67} : the addition of NH_3 caused the mole fraction of CH_4 in the fuel stream to decrease from 1.0 to 0.9 and the decrease of β_{H} (shown in Fig. 8).

In order to clearly show how the NH_3 addition affected the A1 formation pathway, the reactions having an important influence on the formation of species participating in the A1 formation pathway are depicted in Fig. 9 based on results shown in Table 2. Values inside the parentheses represent the $\Delta\gamma/\Delta\gamma_{\text{total}}$ of the reactions. As illustrated, the NH_3 addition to CH_4 flame decreased the A1 formation rate mainly through

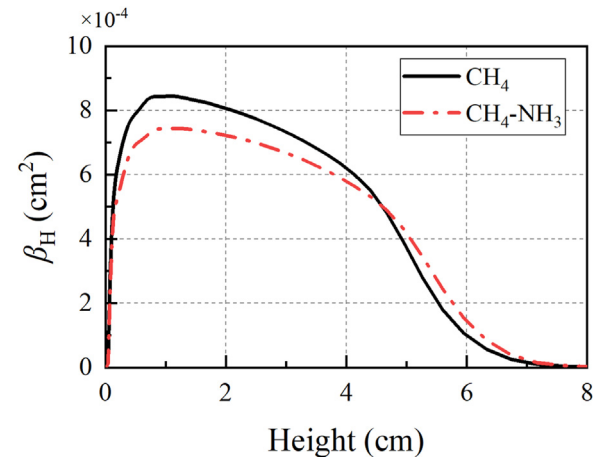
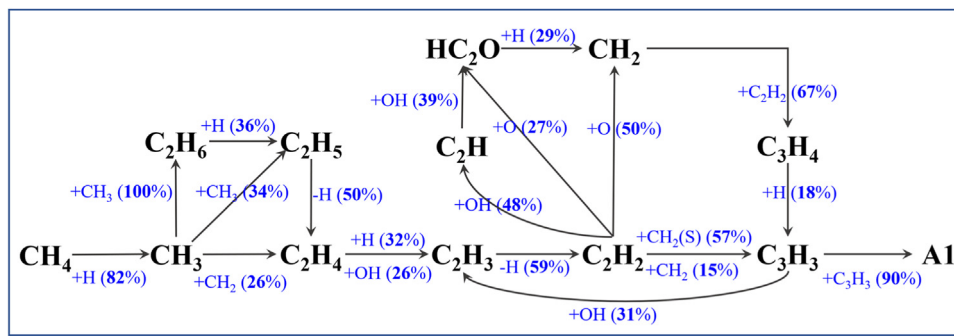


Fig. 8. The distribution of β_{H} of CH_4 and $\text{CH}_4\text{-NH}_3$ flames.

$\text{CH}_4 \rightarrow \text{CH}_3 \rightarrow \text{C}_2\text{H}_6 \rightarrow \text{C}_2\text{H}_5 \rightarrow \text{C}_2\text{H}_4 \rightarrow \text{C}_2\text{H}_3 \rightarrow \text{C}_2\text{H}_2 \rightarrow \text{C}_3\text{H}_3 \rightarrow \text{A1}$ according to the rate of contributions, i.e. $\Delta\gamma/\Delta\gamma_{\text{total}}$ of the reactions. Two other important channels can be found in $\text{CH}_3 \rightarrow \text{C}_2\text{H}_4$ pathway, one was direct formation of C_2H_4 from CH_3 and the other was $\text{CH}_3 \rightarrow \text{C}_2\text{H}_5 \rightarrow \text{C}_2\text{H}_4$. In $\text{C}_2\text{H}_2 \rightarrow \text{C}_3\text{H}_3$ pathway, the C_3H_4 contributed 18% of the decrease in C_3H_3 . Three pathways can be found in $\text{C}_2\text{H}_2 \rightarrow \text{C}_3\text{H}_4$, including $\text{C}_2\text{H}_2 \rightarrow \text{CH}_2 \rightarrow \text{C}_3\text{H}_4$, $\text{C}_2\text{H}_2 \rightarrow \text{C}_2\text{H} \rightarrow \text{HC}_2\text{O} \rightarrow \text{CH}_2 \rightarrow \text{C}_3\text{H}_4$, and $\text{C}_2\text{H}_2 \rightarrow \text{HC}_2\text{O} \rightarrow \text{CH}_2 \rightarrow \text{C}_3\text{H}_4$. In summary, the addition of NH_3 initially resulted in the decrease in CH_3 formation rate mainly through $\text{CH}_4 + \text{H} = \text{CH}_3 + \text{H}_2$ (contributed 82% of CH_3 decrease), and consequently led to the decline of A1 formation through the combination of two C_3H_3 (contributed 90% of A1 decrease).

Fig. 9. The effect of NH_3 addition on the reactions involved in the A1 formation pathway.**Table 3**The integrated rates (γ) of reactions between N-containing and C1~C2 species in the CH_4 and the $\text{CH}_4\text{-NH}_3$ flames.

Species	Chemical Reaction	γ_{CH_4} (mol/s)	$\gamma_{\text{CH}_4\text{-NH}_3}$ (mol/s)	$\Delta\gamma$	$\Delta\gamma/\Delta\gamma_{\text{total}}$
CH_3	R1100: $\text{CH}_3+\text{NH}=\text{CH}_2\text{NH}+H$	6.13×10^{-9}	2.46×10^{-6}	2.45×10^{-6}	42.03
	R1102: $\text{CH}_3+N=\text{H}_2\text{CN}+H$	7.57×10^{-9}	1.03×10^{-6}	1.02×10^{-6}	17.50
$\Delta\gamma_{\text{total}}$:				1.30×10^{-5}	
C_2H_3	R1156: $\text{C}_2\text{H}_3+\text{NO}=\text{HCN}+\text{CH}_2\text{O}$	1.06×10^{-11}	1.09×10^{-9}	1.08×10^{-9}	100
$\Delta\gamma_{\text{total}}$:				1.08×10^{-9}	
C_2H_2	R1159: $\text{C}_2\text{H}_2+\text{NCO}=\text{HC}_2\text{O}+\text{HCN}$	7.91×10^{-10}	8.33×10^{-8}	8.25×10^{-8}	59.56
$\Delta\gamma_{\text{total}}$:				1.39×10^{-7}	
C_2H_5	R1349: $\text{C}_2\text{H}_5+\text{NH}_2(+M)=\text{C}_2\text{H}_5\text{NH}_2(+M)$	4.60×10^{-14}	3.28×10^{-9}	3.28×10^{-9}	57.24
$\Delta\gamma_{\text{total}}$:				5.73×10^{-9}	
C_2H	R1161: $\text{C}_2\text{H}+\text{NO}=\text{HCN}+\text{CO}$	3.40×10^{-8}	2.63×10^{-6}	2.59×10^{-6}	76.64
$\Delta\gamma_{\text{total}}$:				3.38×10^{-6}	
HC_2O	R1171: $\text{HC}_2\text{O}+\text{NO}=\text{HCNO}+\text{CO}$	7.67×10^{-9}	5.81×10^{-7}	5.73×10^{-7}	69.88
$\Delta\gamma_{\text{total}}$:				8.20×10^{-7}	
CH_2	R1114: $\text{CH}_2+\text{NO}=\text{HCNO}+H$	1.64×10^{-8}	1.61×10^{-6}	1.60×10^{-6}	70.20
$\Delta\gamma_{\text{total}}$:				2.28×10^{-6}	

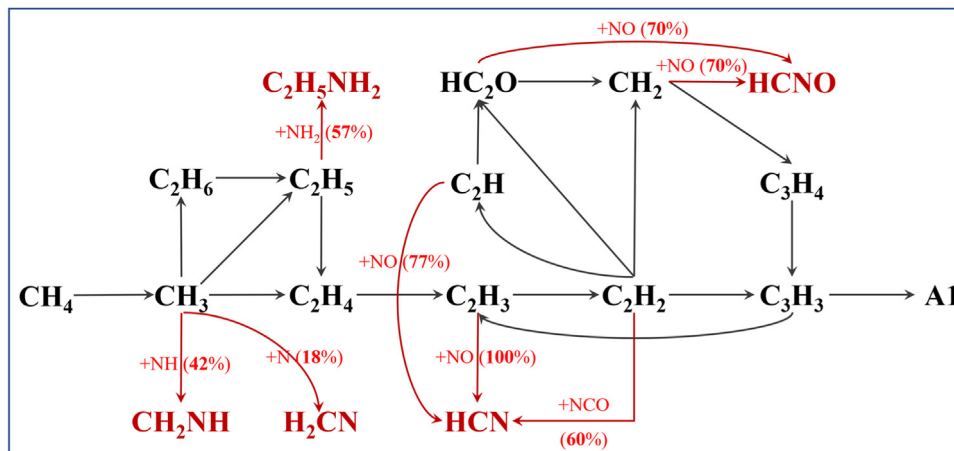


Fig. 10. Reactions between N-containing and C1~C2 species involved in A1 formation.

Overall, the NH_3 addition was found to have significant reduction effect on the formation reaction rates of species participating in the A1 formation pathway. In addition, N-containing species were produced through NH_3 pyrolysis in the $\text{CH}_4\text{-NH}_3$ flame, which reacted with C1~C2 species as shown in Fig. 9. These reactions increased the consumption rates of C1~C2 species and consequently decreased the A1 mole fraction. To quantitatively understand how N-containing species affected the A1 formation pathway, integrated rates of reactions between N-containing and C1~C2 species in the CH_4 and the $\text{CH}_4\text{-NH}_3$ flames were obtained using Eq. (3) and are listed in Table 3. Please note that only the reactions with a relative high ratio of $\Delta\gamma/\Delta\gamma_{\text{total}}$ ($\Delta\gamma = \gamma_{\text{CH}_4\text{-NH}_3} - \gamma_{\text{CH}_4}$) are listed in Table 3. To clearly describe how N-containing

species reacted with the C1~C2 species, related reactions are depicted in Fig. 10, based on Fig. 9 and the data listed in Table 3.

As shown in Table 3, γ of reactions in the $\text{CH}_4\text{-NH}_3$ flame were 2~3 orders higher than those in the CH_4 flame, which confirmed that the NH_3 addition had a significant effect on the consumption of C1~C2 species. As seen in Fig. 10, CH_4 was initially pyrolyzed to CH_3 and C_2H_5 and NH_3 to NH_2 and NH , which provided radical reactants for the reactions between $\text{CH}_3/\text{C}_2\text{H}_5$ and NH_2/NH . While at the later stage, NO dominated the N-related reactions with C_2H_3 , C_2H , HC_2O and CH_2 .

As shown in Figs. 9 and 10, along the main formation pathway of A1 ($\text{CH}_4 \rightarrow \text{CH}_3 \rightarrow \text{C}_2\text{H}_6 \rightarrow \text{C}_2\text{H}_5 \rightarrow \text{C}_2\text{H}_4 \rightarrow \text{C}_2\text{H}_3 \rightarrow \text{C}_2\text{H}_2 \rightarrow \text{C}_3\text{H}_3 \rightarrow \text{A1}$), N-containing species primarily react with CH_3 , C_2H_5 , C_2H_3 and C_2H_2 . Compared to the CH_4 flame, γ_{R1100} in the

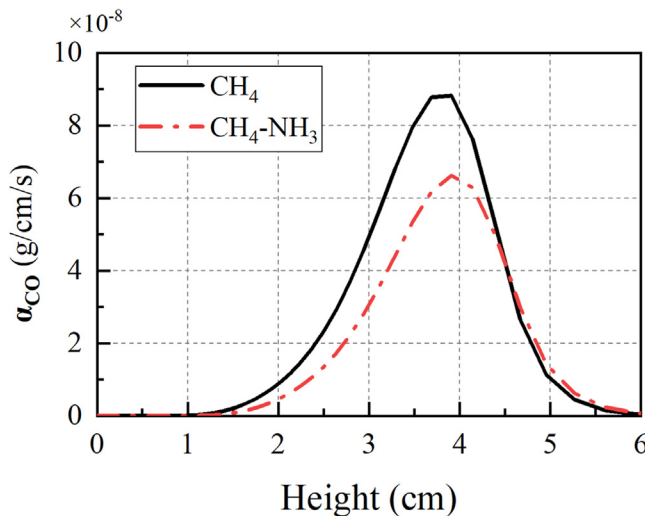


Fig. 11. Distribution of α_{CO} of the CH_4 and the $\text{CH}_4\text{-NH}_3$ flames.

$\text{CH}_4\text{-NH}_3$ flame increased by 2.45×10^{-6} mol/s, which played the most important role in the increase of CH_3 consumption. In addition, the N-substitution reaction of CH_3 (R1102: $\text{CH}_3 + \text{N} = \text{H}_2\text{CN} + \text{H}$) also had a vital impact on the increase of CH_3 consumption, with γ_{R1102} increasing from 7.57×10^{-9} to 1.03×10^{-6} mol/s. The increase in C_2H_5 consumption was due to the increase of γ_{R1349} from 4.60×10^{-14} mol/s in the CH_4 flame to 3.28×10^{-9} mol/s in the $\text{CH}_4\text{-NH}_3$ flame. The increase of C_2H_3 consumption in the $\text{CH}_4\text{-NH}_3$ flame compared to the CH_4 flame was attributed to the increase of γ_{R1156} from 1.06×10^{-11} to 1.09×10^{-9} mol/s, with $\Delta\gamma/\Delta\gamma_{total}$ of around 100%. The increase of γ_{R1159} ($\text{C}_2\text{H}_2 + \text{NCO} = \text{HC}_2\text{O} + \text{HCN}$) from 7.91×10^{-10} mol/s in the CH_4 flame to 8.33×10^{-8} mol/s in the $\text{CH}_4\text{-NH}_3$ flame played a crucial role in the increase of C_2H_2 consumption.

In the branched formation pathway of A1 shown in Fig. 10, two main N-containing species contributed to the consumption of CH_2 , HC_2O and C_2H in the $\text{CH}_4\text{-NH}_3$ flame, namely NO and NH_2 . The increase in C_2H consumption was primarily due to the increase of γ_{R1161} ($\text{C}_2\text{H} + \text{NO} = \text{HCN} + \text{CO}$, by 2.59×10^{-6} mol/s). As shown in Table 3, the NH_3 addition increased γ_{R1171} ($\text{HC}_2\text{O} + \text{NO} = \text{HCNO} + \text{CO}$) and γ_{R1114} ($\text{CH}_2 + \text{NO} = \text{HCNO} + \text{H}$) by 5.73×10^{-7} and 1.60×10^{-6} mol/s, respectively, which increased HC_2O and CH_2 consumption.

4.1.2. on soot condensation and HACA surface growth

Once the initial soot particles were formed through the collision between two A5s, the subsequent increase of soot mass primarily came from PAH condensation and the HACA surface growth mechanism [38]. As shown in Fig. 11, the α_{CO} obviously decreased as NH_3 was added to the CH_4 flame. The peak α_{CO} was 8.82×10^{-8} g/cm/s in the CH_4 flame and it dropped to 6.62×10^{-8} g/cm/s in the $\text{CH}_4\text{-NH}_3$ flame. The PAH condensation process was modelled as the collision between soot and A5s. As a result, it depends on temperature, and A5 and soot concentrations. It is observed from Fig. 3(a-b) that the addition of NH_3 to the CH_4 flame led to a decrease in the peak temperature by ~ 4 K, which contributed minorly to the decline of the PAH condensation rate. As illustrated above (see Fig. 6), the NH_3 addition decreased the peak β_{BGHIF} and β_{BAPYR} by 6.62% and 14.4%, which consequently decreased the condensation rate. As shown in Fig. 5, the NH_3 addition resulted in a decrease of peak α_{IN} by 13.7%, which subsequently lowered the condensation rate.

The α_{HACA} distributions of the CH_4 and the $\text{CH}_4\text{-NH}_3$ flames are plotted in Fig. 12. By comparing the results in Figs. 5, 11 and

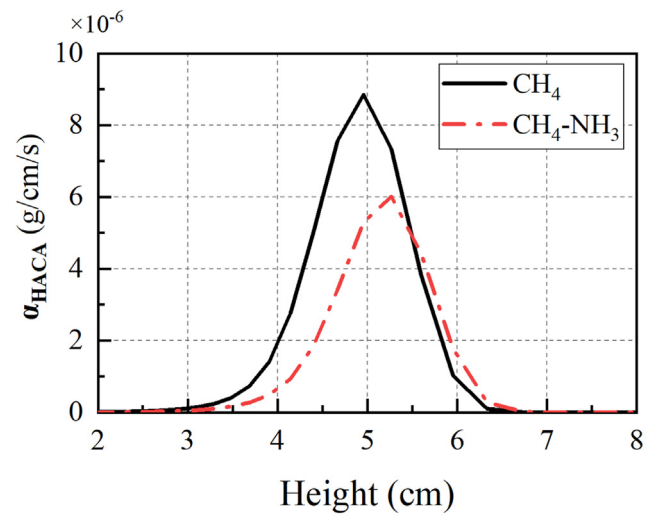


Fig. 12. The distribution of α_{HACA} of CH_4 and $\text{CH}_4\text{-NH}_3$ flames.

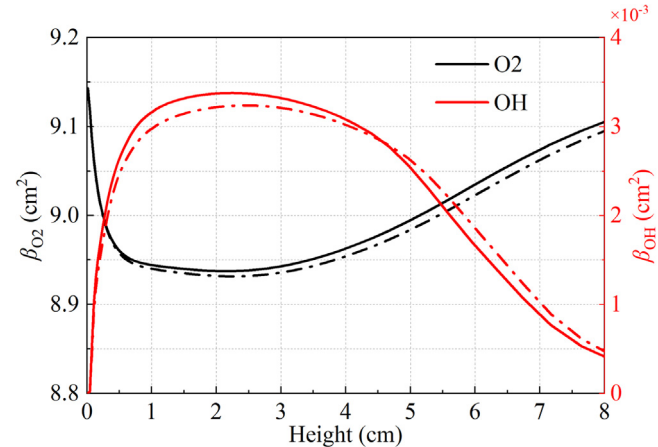


Fig. 13. The distributions of β_H and β_{OH} , the solid line represents the β of CH_4 flame and dot dash line represents the β of $\text{CH}_4\text{-NH}_3$ flame.

12, we can find that α_{HACA} was around two orders of magnitude higher than α_{IN} and α_{CO} and it contributed the most to soot formation. In the CH_4 flame, the peak α_{HACA} was 8.85×10^{-6} g/cm/s and it decreased to 6.01×10^{-6} g/cm/s in the $\text{CH}_4\text{-NH}_3$ flame, with a drop of 32.1%. The HACA surface growth rate mainly depends on the C_2H_2 concentration, the number of dehydrogenated sites on the soot surface ($\chi_{\text{C-soot}\star}$) and soot concentration [38]. As shown in Fig. 12, the HACA surface growth occurred at the height of 3~6 cm of the CH_4 flame and dramatically decreased in the height of 3~5 cm when NH_3 was added. Figure 4(d) shows that the NH_3 addition led to $\beta_{C_2H_2}$ at $z = 3\text{--}5$ cm increasing slightly, an opposite trend compared to the change of HACA surface growth. This indicated that the change of C_2H_2 had a limited effect on the decrease in HACA surface growth rate. $\chi_{\text{C-soot}\star}$ has a positive relation with H , OH and soot concentrations [38]. When NH_3 was added to the CH_4 flame, β_H and β_{OH} at the height of 3~4.5 cm decreased (see Fig. 8 and 13), which is consistent with the declining trend of HACA surface growth. That meant H and OH played important roles in the decrease of HACA surface growth. As mentioned above, the NH_3 addition lowered the soot inception and condensation rate, which resulted in the decrease of soot concentration, and consequently reduced the HACA surface growth rate.

4.1.3. on soot oxidation

The soot oxidation processes include reactions with O_2 and OH . O_2 oxidation was modelled using the HACA mechanism and OH

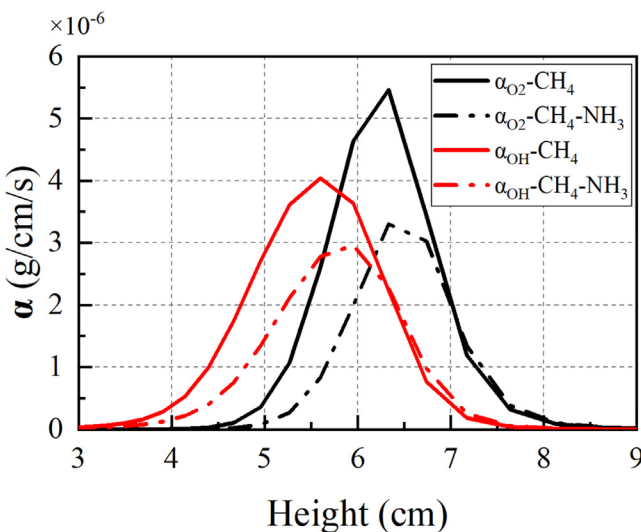


Fig. 14. The distribution of α_{O_2} and α_{OH} of CH_4 and $CH_4\text{-NH}_3$ flames.

oxidation as collisions between OH radical and soot particles. As shown in Fig. 14, the OH oxidation process started at the height of 3 cm while the O₂ oxidation process started at the height of around 5 cm. They both vanished at the height of around 8 cm. Fig. 14 also shows both α_{O_2} and α_{OH} decreased with NH₃ addition. Comparing the two soot oxidation processes, the decrease in α_{O_2} was 2.16×10^{-6} g/mol/s, which was twice larger than that of α_{OH} (1.08×10^{-6} g/mol/s). The O₂ and OH oxidation processes depend on two major factors: one is O₂ and OH concentrations, respectively, and the other is soot concentration. The maximum decrease in β_{O_2} and β_{OH} shown in Fig. 13 are 0.13% and 4.1%, which are obviously lower than those of α_{O_2} (39.5%) and α_{OH} (26.8%). This implies the change of O₂ and OH mole fraction were not the major source of influence on the decrease in O₂ and OH oxidation. It can thus be concluded that the decrease of soot concentration through inception, condensation and HACA surface growth were vital for the decrease in O₂ and OH oxidation rates in the $CH_4\text{-NH}_3$ flame.

4.1.4. Comparison of soot formation in $CH_4\text{-NH}_3$ and $C_2H_4\text{-NH}_3$ flames

In order to investigate the effect of NH₃ addition on the soot formation in different hydrocarbon fuel flames, normalized maximal PAHs/soot mole fractions along the centerline of the $CH_4\text{-NH}_3$ flames in this study were compared with those of $C_2H_4\text{-NH}_3$ flames in [11] and [39]. As shown in Fig. 15, the PAHs and soot

formation was dramatically suppressed by NH₃ in both CH_4 and C_2H_4 flames. As the ring number of PAH molecules increased, such inhibiting effect of NH₃ on PAHs formation became stronger.

The main formation pathway of A1 in $C_2H_4\text{-NH}_3$ flames [39] is $C_2H_4 \rightarrow C_2H_3 \rightarrow C_2H_2 \rightarrow C_3H_3 \rightarrow A1$, which is the same as the latter part of the main A1 formation pathway in $CH_4\text{-NH}_3$ flames ($CH_4 \rightarrow CH_3 \rightarrow C_2H_6 \rightarrow C_2H_5 \rightarrow C_2H_4 \rightarrow C_2H_3 \rightarrow C_2H_2 \rightarrow C_3H_3 \rightarrow A1$). In the $C_2H_4\text{-NH}_3$ flames of [39], the formation of C_2H_2 and C_3H_3 was suppressed by NH₃, which was responsible for the reduced A1 generation rate. In $CH_4\text{-NH}_3$ flame, besides C_2H_2 and C_3H_3 , the formation of C_2H_5 and C_2H_6 was also limited and played a key role in the decrease of the A1 mole fraction. It is clear from Fig. 10 that many CN species, such as CH_2NH , H_2CH and CH_2CN , were produced via the nitrogen-hydrocarbon interactions, which blocked the formation of hydrocarbon radicals (C_2H_2 , C_2H_5 , C_2H_6 , C_3H_3). Similarly, the formation of CN species (CH_2CHNH_2 , CH_3NH_2 , CH_2NH , HCN , etc.) was considered the cause of the decrease of C_2H_2 and C_3H_3 concentrations in $C_2H_4\text{-NH}_3$ flames of [39].

4.2. Effects of NH₃ addition on NO and N₂O formation

4.2.1. On NO formation

Although NH₃ addition in the fuel stream of CH_4 or other hydrocarbons suppresses soot formation, a major potential penalty is increased NO emission. Hence, in this section the effect of NH₃ addition on NO emission is discussed. Predicted NO distributions of the two cases are depicted in Fig. 16. It is obvious that the NO formation in the $CH_4\text{-NH}_3$ flame was two orders of magnitude higher than that in the CH_4 flame. The location of maximum NO in CH_4 flame appeared in the high-temperature region at higher elevations, while in the $CH_4\text{-NH}_3$ flame it occurred at a much lower height of ~ 0.2 cm, slightly above the burner exit. The dramatically higher NO amount in the $CH_4\text{-NH}_3$ flame revealed a significant impact of NH₃ addition on NO formation.

It is established that NO species are formed through thermal, prompt and fuel routes [40]. In hydrocarbon flames, thermal and prompt routes dominate and the fuel route is typically negligible. In contrast, the tremendously increased NO formation in $CH_4\text{-NH}_3$ flame was due to the NH₃ addition in the fuel stream, i.e., through the fuel route. The major reactions that participated in the NO formation of the CH_4 and the $CH_4\text{-NH}_3$ flames and the integrated rates over the whole computational domain are listed in supplemental material (integrated reaction rates of CH_4 and $CH_4\text{-NH}_3$ flames.xlsx) and a diagram of the reaction pathways are provided in Fig. 17. As illustrated in Fig. 17, the major reactions affecting NO formation at the selected elevation were increased by 2 orders of magnitude due to the NH₃ addition. In the CH_4 flame, the most important NO formation channel was R849 ($N+OH=NO+H$) and

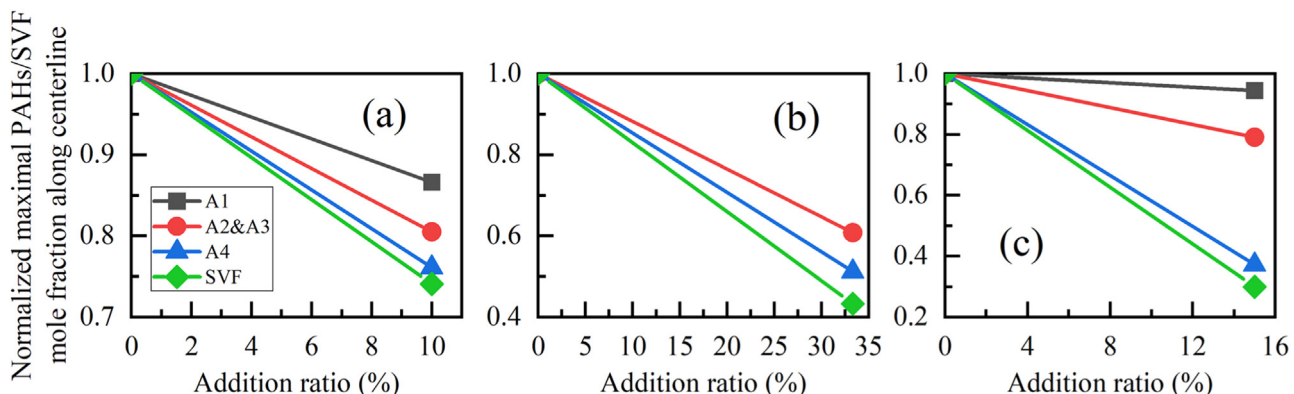


Fig. 15. Normalized maximal PAHs/soot mole fractions along centerline in (a) the $CH_4\text{-NH}_3$ flames investigated in this study, (b) the $C_2H_4\text{-NH}_3$ flames in [11] and (c) the $C_2H_4\text{-NH}_3$ flame in [39].

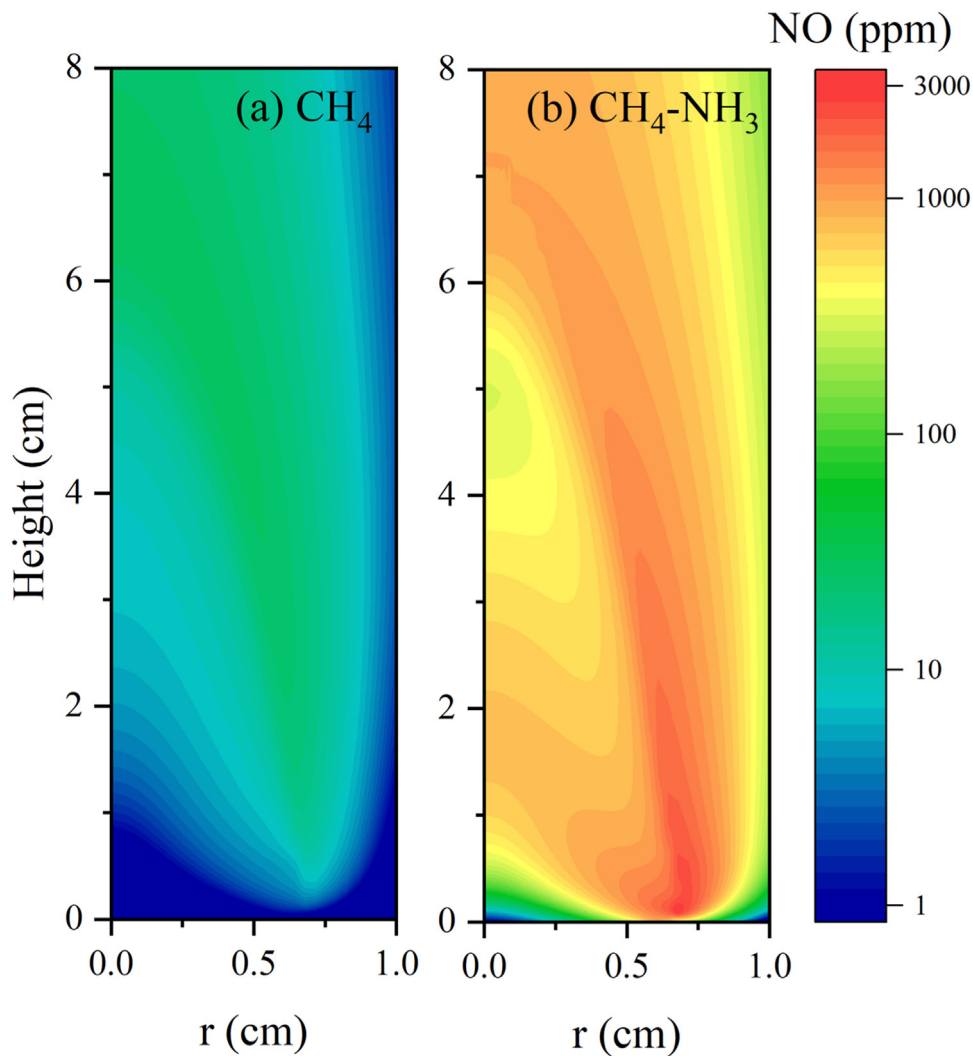


Fig. 16. NO distributions of (a) the CH_4 and (b) the $\text{CH}_4\text{-NH}_3$ flames. Peak fractions are 28 and 3060 ppm for the CH_4 and the $\text{CH}_4\text{-NH}_3$ flames, respectively.

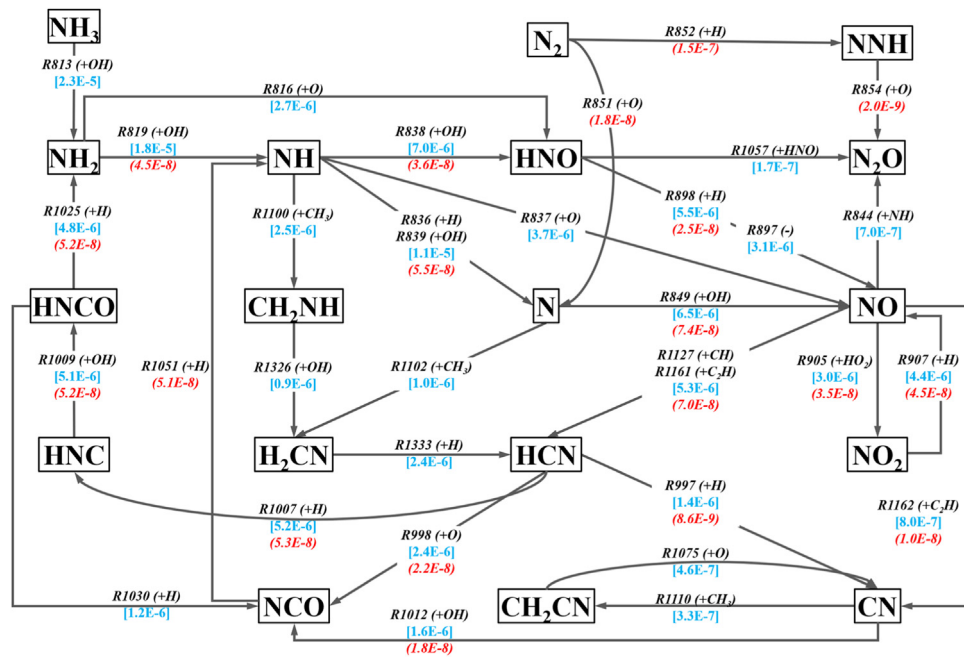


Fig. 17. Reaction pathways of NO and N_2O formation of the CH_4 and the $\text{CH}_4\text{-NH}_3$ flames. The red numbers in parenthesis and blue numbers in square brackets are integrated reaction rates in the CH_4 and the $\text{CH}_4\text{-NH}_3$ flames, respectively.

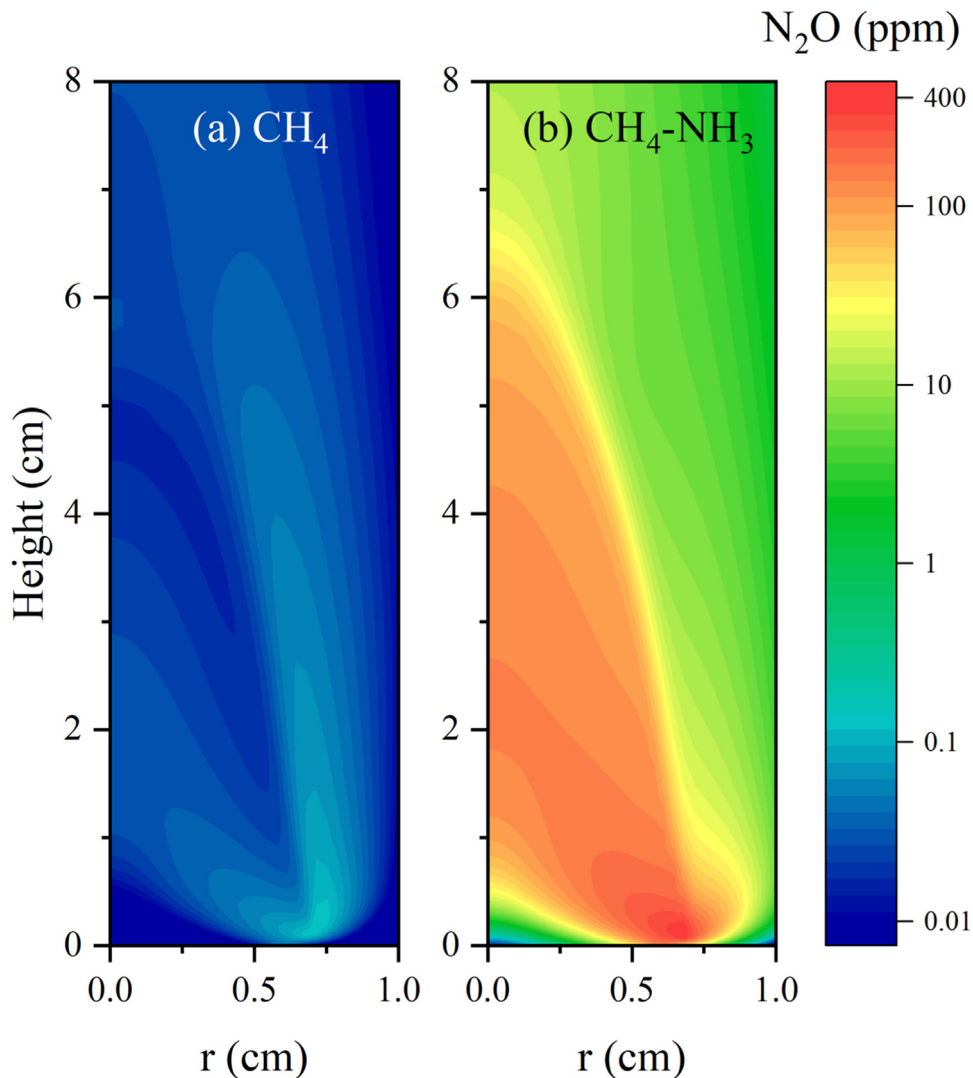


Fig. 18. N₂O distributions of (a) the CH₄ and (b) the CH₄-NH₃ flames. Peak fractions are 0.15 and 399 ppm in the CH₄ and the CH₄-NH₃ flames, respectively.

the second was R898 (HNO+H=NO+H₂). In the CH₄-NH₃ flame, two orders of magnitude increase in γ_{R849} and γ_{R898} were attained, which were mainly responsible for the increase of NO formation. While besides the above two paths, R837 (NH+O=NO+H) and R897 (HNO(+M)=NO+H(+M)) also played important roles in the increase of NO formation, with a γ of 3.7×10^{-6} and 3.1×10^{-6} mol/s, respectively. The most important precursor participating in NO formation was N radical in CH₄ flame, while it was HNO in CH₄-NH₃ flame since HNO was the reactant of R898 and R897. The total integral conversion rate from HNO to NO was 8.6×10^{-6} mol/s.

As shown in Fig. 17, the initiation reaction in the CH₄ flame was the O radical's attack on the triple bonds in N₂ (R851: N₂+O = N+NO), but in the CH₄-NH₃ flame the initial step was the decomposition of NH₃ via R813 (NH₃+OH=NH₂+H₂O). It is evident that the NH₃ addition in the CH₄ flame made the reactions between C1~C2 and N-containing species more vigorous, and consequently more CN species. For example, the NH₃ addition increased γ_{R1127} (CH+NO=HCN+O) and γ_{R1161} (C₂H+NO=HCN+CO) to 5.3×10^{-6} mol/s, which contributed the most to the increase of HCN formation in the CH₄-NH₃ flame. Two new HCN formation pathways can be found in Fig. 17 due to the addition of NH₃: NH₃→NH₂→NH→CH₂NH→H₂CN→HCN and NH₃→NH₂→NH→N→H₂CN→HCN. The CN formation rate was

then enhanced due to the increase of γ_{R997} to 1.4×10^{-6} mol/s. Moreover, R1162 (C₂H+NO=CN+HCO) also played a key role in the increase of CN formation, whose γ increased from 1.0×10^{-8} mol/s in the CH₄ flame to 8.0×10^{-7} mol/s in the CH₄-NH₃ flame.

Moreover, the literature on coal/char combustion has established that NO reduction occurs by char [41,42]. However, it is reasonable to presume that the NO reduction by soot in the CH₄-NH₃ flame is limited as reflected by the SVF and NO distributions showed in Figs. 4(b) and 16(b). Firstly, the maximal SVF of the CH₄-NH₃ flame was less than 0.1 ppm, which was four orders of magnitude smaller than the maximal NO concentration (~ 3000 ppm). Secondly, it is clear that the soot is mainly generated at the height of 5~6 cm and close to the flame centerline, where the NO concentration was lower than 700 ppm. Therefore, due to huge concentration differentials and the different distributions between NO and soot, the NO reduction by soot is deemed limited.

4.2.2. On N₂O formation

Besides NO, N₂O is also an important nitrogen oxide which is a particularly potent greenhouse species [43]. Predicted N₂O distributions of the CH₄ and CH₄-NH₃ flames are depicted in Fig. 18. It is clear that the N₂O mole fractions of the CH₄-NH₃ flame were

remarkably higher than those of the CH₄ flame, indicating a facilitating effect of the NH₃ addition on N₂O formation, similar to that on NO although its concentration in the CH₄-NH₃ case was an order of magnitude lower.

The N₂O formation pathways of the CH₄ and the CH₄-NH₃ flames are displayed in Fig. 17. In the CH₄ flame, N₂O was mainly produced through the oxidation of NNH (R854: NNH+O = N₂O+H) with a γ of 2.0×10^{-9} mol/s, and NNH was primarily generated via R852 (N₂+H=NNH). Most NNH was consumed via R858 (NNH+O₂=N₂+HO₂), which resulted in a low mole fraction of N₂O. In contrast, different N₂O formation pathways were found in the CH₄-NH₃ flame, where N₂O was mainly produced through R844 (NH+NO=N₂O+H with a γ of 7.0×10^{-7} mol/s) and R1057 (HNO+HNO=N₂O+H₂O, $\gamma = 1.7 \times 10^{-7}$ mol/s). Both γ_{R844} and γ_{R1057} in the CH₄-NH₃ flame were about two orders of magnitude larger than γ_{R854} in CH₄ flame, which explained the reason for the obvious higher mole fraction of N₂O in CH₄-NH₃ flame.

5. Conclusion

The effects of NH₃ addition in the fuel stream on soot and NO formation in a CH₄/air co-flow atmospheric-pressure diffusion flame were numerically investigated using a 2D code and a detailed chemical reaction mechanism that contains reactions for both soot and NO formation. The integral of reaction rates over the whole flame were obtained in both CH₄ and CH₄-NH₃ flames to quantitatively investigate how the NH₃ addition affected the soot and NO formation pathways. The reactions between C1~C2 species and N-containing species were considered in the soot and NO formation pathways. Several conclusions can be drawn from this study as follows.

- 1) NH₃ addition to the CH₄ diffusion flame had a strong suppression on soot formation, reducing peak SVF by 38.9%, but dramatically promoted NO production and led to an increase of peak NO by two orders of magnitude. As for flame temperature, the NH₃ addition led to a minor decrease in the maximum temperature by 4.1 K.
- 2) NH₃ addition contributed to the decrease of the integrated reaction rate of R67 (CH₄+H=CH₃+H₂) by 1.07×10^{-5} mol/s, which consequently decreased the A1 formation rate through the pathway of CH₄→CH₃→C₂H₆→C₂H₅→C₂H₄→C₂H₃→C₂H₂→C₃H₃→A1. NO and NH played a significant role in the consumption of C1~C2 species involved in A1 formation. The NH₃ addition resulted in an increase in the integrated rates of CH₃+NH=CH₂NH+H and C₂H+NO=HCN+CO by 2.45×10^{-6} and 2.59×10^{-6} mol/s, respectively, which ultimately decreased the A5 formation and soot inception rates.
- 3) The decrease in inception rate played the most important role in reducing the condensation, the HACA surface growth and the O₂/OH oxidation rates. In addition, the decrease in condensation rate was partly due to the decrease in BGHIF and BAPYR mole fractions. The drop in OH mole fraction also had some effect on the decrease of HACA surface growth, and O₂ and OH oxidation rates.
- 4) The integrated reaction rates in NO formation pathways were increased by two orders of magnitude with NH₃ addition. Compared to the CH₄ flame, more channels for NO formation can be found and more CN species were produced in the CH₄-NH₃ flame. Similar to NO formation, a promoting effect of NH₃ addition on N₂O was observed. However, the N₂O formation in the two cases were through completely different channels - via NNH in the CH₄ case and via HNO/NO in the CH₄-NH₃ case.

Declaration of Competing Interest

The authors declare that they have no known competing financial interests or personal relationships that could have appeared to influence the work reported in this paper.

Acknowledgements

This research was supported by the National Natural Science Foundation of China (Nos. 52276185, 51976057, 51922040 and 52206157) and the Fundamental Research Funds for the Central Universities (Nos. 2020JG005 and 2020DF01). RS in addition acknowledges support from NSFC through a National Talent Program.

Supplementary materials

Supplementary material associated with this article can be found, in the online version, at doi:[10.1016/j.combustflame.2022.112483](https://doi.org/10.1016/j.combustflame.2022.112483).

References

- [1] H. Kobayashi, A. Hayakawa, K. Somaratne, E. Okafor, Science and technology of ammonia combustion, Proc. Combust. Inst. 37 (1) (2019) 109–133.
- [2] A. Valera-Medina, F. Amer-Hatem, A.K. Azad, I.C. Dedoussi, M. Costa, Review on ammonia as a potential fuel: from synthesis to economics, Energy Fuels (2021).
- [3] X. Han, Z. Wang, M. Costa, Z. Sun, K. Cen, Experimental and kinetic modeling study of laminar burning velocities of NH₃/air, NH₃/H₂/air, NH₃/CO/air and NH₃/CH₄/air premixed flames, Combust. Flame 206 (2019) 214–226.
- [4] C. Zamfirescu, I. Dincer, Ammonia as a green fuel and hydrogen source for vehicular applications, Fuel Process. Technol. 90 (5) (2009) 729–737.
- [5] J.W. Ku, S. Choi, H.K. Kim, S. Lee, O.C. Kwon, Extinction limits and structure of counterflow nonpremixed methane-ammonia/air flames, Energy 165 (2018) 314–325.
- [6] E.C. Okafor, Y. Naito, S. Colson, A. Ichikawa, T. Kudo, A. Hayakawa, H. Kobayashi, Experimental and numerical study of the laminar burning velocity of CH₄-NH₃-air premixed flames, Combust. Flame 187 (2018) 185–198.
- [7] O. Kurata, N. Iki, T. Matsunuma, T. Inoue, T. Tsujimura, H. Furutani, H. Kobayashi, A. Hayakawa, Performances and emission characteristics of NH₃-air and NH₃CH₄-air combustion gas-turbine power generations, Proc. Combust. Inst. 36 (3) (2017) 3351–3359.
- [8] H. Bockhorn, F. Fetting, U. Meyer, R. Reck, G. Wannemacher, Measurement of the soot concentration and soot particle sizes in propane oxygen flames, Symp. Combust. 18 (1) (1981) 1137–1147.
- [9] A.M. Bennett, P. Liu, Z. Li, N.M. Kharbatia, W. Boyette, A.R. Masri, W.L. Roberts, Soot formation in laminar flames of ethylene/ammonia, Combust. Flame 220 (2020) 210–218.
- [10] M.J. Montgomery, H. Kwon, J.A.H. Dreyer, Y. Xuan, C.S. McEnally, L.D. Pfefferle, Effect of ammonia addition on suppressing soot formation in methane co-flow diffusion flames, Proc. Combust. Inst. 38 (2) (2021) 2497–2505.
- [11] Y. Liu, X. Cheng, Y. Li, L. Qiu, X. Wang, Y. Xu, Effects of ammonia addition on soot formation in ethylene laminar diffusion flames, Fuel 292 (2021) 120416.
- [12] L. Bo, H. Yong, Z. Li, A.A. Konnov, Measurements of NO concentration in NH₃-doped CH₄ + air flames using saturated laser-induced fluorescence and probe sampling, Combust. Flame 160 (1) (2013) 40–46.
- [13] H. Xiao, S. Lai, A. Valera-Medina, J. Li, J. Liu, H. Fu, Study on counterflow premixed flames using high concentration ammonia mixed with methane, Fuel 275 (2020) 117902.
- [14] N. Sullivan, A. Jensen, P. Glarborg, M.S. Day, J.F. Grcar, J.B. Bell, C.J. Pope, R.J. Kee, Ammonia conversion and NO_x formation in laminar coflowing non-premixed methane-air flames, Combust. Flame 131 (3) (2002) 285–298.
- [15] M. Woo, B.C. Choi, A.F. Ghoniem, Experimental and numerical studies on NO_x emission characteristics in laminar non-premixed jet flames of ammonia-containing methane fuel with oxygen/nitrogen oxidizer, Energy 114 (2016) 961–972.
- [16] H. Guo, G.J. Smallwood, The interaction between soot and NO formation in a laminar axisymmetric coflow ethylene/air diffusion flame, Combust. Flame 149 (1–2) (2007) 225–233.
- [17] N.A. Eaves, Q. Zhang, F. Liu, H. Guo, S.B. Dworkin, M.J. Thomson, CoFlame: a refined and validated numerical algorithm for modeling sooting laminar coflow diffusion flames, Comput. Phys. Commun. (2016) 464–477.
- [18] Q. Zhang, Detailed Modeling of Soot Formation/Oxidation in Laminar Coflow Diffusion Flames, University of Toronto (Canada), 2009 PhD thesis.
- [19] S.B. Dworkin, Q. Zhang, M.J. Thomson, N.A. Slavinskaya, U. Riedel, Application of an enhanced PAH growth model to soot formation in a laminar coflow ethylene/air diffusion flame, Combust. Flame 158 (9) (2011) 1682–1695.
- [20] J. Appel, H. Bockhorn, M. Frenklach, Kinetic modeling of soot formation with detailed chemistry and physics: laminar premixed flames of C2 hydrocarbons, Combust. Flame 121 (1–2) (2000) 122–136.

- [21] F. Liu, S.B. Dworkin, M.J. Thomson, G.J. Smallwood, Modeling DME addition effects to fuel on PAH and soot in laminar coflow ethylene/air diffusion flames using two PAH mechanisms, *Combust. Sci. Technol.* 184 (7–9) (2012) 966–979.
- [22] F. Liu, Y. Ai, W. Kong, Effect of hydrogen and helium addition to fuel on soot formation in an axisymmetric coflow laminar methane/air diffusion flame, *Int. J. Hydrogen Energy* 39 (8) (2014) 3936–3946.
- [23] S. Park, S. Rogak, W. Bushe, Z. Wen, M. Thomson, An aerosol model to predict size and structure of soot particles, *J. Aerosol Sci.* 35 (2004) S825–S826.
- [24] Q. Zhang, M.J. Thomson, H. Guo, F. Liu, G.J. Smallwood, Modeling of oxidation-driven soot aggregate fragmentation in a laminar coflow diffusion flame, *Combust. Sci. Technol.* 182 (4–6) (2010) 491–504.
- [25] P. Glarborg, J.A. Miller, B. Ruscic, S.J. Klippenstein, Modeling nitrogen chemistry in combustion, *Prog. Energy Combust. Sci.* 67 (2018) 31–68.
- [26] V. Chernov, M.J. Thomson, S.B. Dworkin, N.A. Slavinskaya, U. Riedel, Soot formation with C1 and C2 fuels using an improved chemical mechanism for PAH growth, *Combust. Flame* 161 (2) (2014) 592–601.
- [27] L. Dai, S. Gersen, P. Glarborg, A. Mokhov, H. Levinsky, Autoignition studies of NH₃/CH₄ mixtures at high pressure, *Combust. Flame* 218 (2020) 19–26.
- [28] S. Steinmetz, H. Ahmed, W. Boyette, M. Dunn, W.L. Roberts, A. Masri, Effects of ammonia and hydrogen on the sooting characteristics of laminar coflow flames of ethylene and methane, *Fuel* 307 (2022) 121914.
- [29] R.C. Rocha, S. Zhong, L. Xu, X.-S. Bai, M. Costa, X. Cai, H. Kim, C. Brackmann, Z. Li, M. Alden, Structure and laminar flame speed of an ammonia/methane/air premixed flame under varying pressure and equivalence ratio, *Energy Fuels* 35 (9) (2021) 7179–7192.
- [30] S. Arunthanayothin, A. Stagni, Y. Song, O. Herbinet, T. Faravelli, F. Battin-Leclerc, Ammonia–methane interaction in jet-stirred and flow reactors: an experimental and kinetic modeling study, *Proc. Combust. Inst.* 38 (1) (2021) 345–353.
- [31] A. Stagni, C. Cavallotti, S. Arunthanayothin, Y. Song, O. Herbinet, F. Battin-Leclerc, T. Faravelli, An experimental, theoretical and kinetic-modeling study of the gas-phase oxidation of ammonia, *React. Chem. Eng.* 5 (4) (2020) 696–711.
- [32] F. Liu, G.J. Smallwood, m.L. Gülder, Application of the statistical narrow-band correlated-k method to low-resolution spectral intensity and radiative heat transfer calculations – effects of the quadrature scheme, *Int. J. Heat Mass Transf.* 43 (17) (2000) 3119–3135.
- [33] F. Liu, H. Guo, G.J. Smallwood, Effects of radiation model on the modeling of a laminar coflow methane/air diffusion flame, *Combust. Flame* 138 (1–2) (2004) 136–154.
- [34] C. Thurgood, A. Pollard, H. Becker, The TN quadrature set for the discrete ordinates method, *J. Heat Transf.* 117 (4) (1995) 1068–1070.
- [35] S. Zheng, R. Sui, W. Liang, H. Zhou, C.K. Law, On band lumping, radiation reabsorption, and high-pressure effects in laminar flame propagation, *Combust. Flame* 221 (2020) 86–93.
- [36] S. Zheng, Y. Yang, R. Sui, Q. Lu, Effects of C₂H₂ and C₂H₄ radiation on soot formation in ethylene/air diffusion flames, *Appl. Therm. Eng.* 183 (2021) 116194.
- [37] M. Smooke, C. McEnally, L. Pfefferle, R. Hall, M. Colket, Computational and experimental study of soot formation in a coflow, laminar diffusion flame, *Combust. Flame* 117 (1–2) (1999) 117–139.
- [38] A. Jerez, J.-L. Consalvi, A. Fuentes, F. Liu, R. Demarco, Soot production modeling in a laminar coflow ethylene diffusion flame at different Oxygen Indices using a PAH-based sectional model, *Fuel* 231 (2018) 404–416.
- [39] F. Ren, X. Cheng, Z. Gao, Z. Huang, L. Zhu, Effects of NH₃ addition on polycyclic aromatic hydrocarbon and soot formation in C₂H₄ co-flow diffusion flames, *Combust. Flame* 241 (2022) 111958.
- [40] J.A. Miller, C.T. Bowman, Mechanism and modeling of nitrogen chemistry in combustion, *Prog. Energy Combust. Sci.* 15 (4) (1989) 287–338.
- [41] C. Arnal, M. Alzueta, A. Millera, R. Bilbao, Experimental and kinetic study of the interaction of a commercial soot with NO at high temperature, *Combust. Sci. Technol.* 184 (7–8) (2012) 1191–1206.
- [42] T. Mendiara, M. Alzueta, A. Millera, R. Bilbao, Influence of the NO concentration and the presence of oxygen in the acetylene soot reaction with NO, *Energy Fuels* 22 (1) (2008) 284–290.
- [43] A. Hayakawa, M. Hayashi, G. Gotama, M. Kovaleva, E. Okafor, S. Colson, S. Mashruk, A. Valera Medina, H. Kobayashi, N₂O production characteristics of strain stabilized premixed laminar ammonia/hydrogen/air premixed flames in lean conditions, (2021)